Biochemical and Biophysical Research Communications 446 (2014) 911–915

Contents lists available at ScienceDirect

Biochemical and Biophysical Research Communications

journal homepage: www.elsevier.com/locate/ybbrc

Structural basis for high substrate-binding affinity and enantioselectivity of 3-quinuclidinone reductase AtQR

Feng Hou [a], Takuya Miyakawa [a], Michihiko Kataoka [b,c], Daijiro Takeshita [a], Shoko Kumashiro [c], Atsuko Uzura [d], Nobuyuki Urano [b,c], Koji Nagata [a], Sakayu Shimizu [c,e], Masaru Tanokura [a,*]

[a] Department of Applied Biological Chemistry, Graduate School of Agricultural and Life Sciences, The University of Tokyo, 1-1-1 Yayoi, Bunkyo-ku, Tokyo 113-8657, Japan
[b] Division of Applied Life Sciences, Graduate School of Life and Environmental Sciences, Osaka Prefecture University, 1-1 Gakuen-cho, Naka-ku, Sakai 559-8531, Japan
[c] Division of Applied Life Sciences, Graduate School of Agriculture, Kyoto University, Kitashirakawa-Oiwakecho, Sakyo-ku, Kyoto 606-8502, Japan
[d] Research & Development Center, Nagase & Co., Ltd., 2-2-3 Muratani, Nishi-ku, Kobe 651-2241, Japan
[e] Faculty of Bioenvironmental Science, Kyoto Gakuen University, Sogabe-cho, Kameoka 621-8555, Japan

ARTICLE INFO

Article history:
Received 5 March 2014
Available online 15 March 2014

Keywords:
Crystal structure
Short-chain dehydrogenases/reductases
Quinuclidinone
Agrobacterium tumefaciens

ABSTRACT

(*R*)-3-Quinuclidinol, a useful compound for the synthesis of various pharmaceuticals, can be enantioselectively produced from 3-quinuclidinone by 3-quinuclidinone reductase. Recently, a novel NADH-dependent 3-quinuclidionone reductase (AtQR) was isolated from *Agrobacterium tumefaciens*, and showed much higher substrate-binding affinity (>100 fold) than the reported 3-quinuclidionone reductase (RrQR) from *Rhodotorula rubra*. Here, we report the crystal structure of AtQR at 1.72 Å. Three NADH-bound protomers and one NADH-free protomer form a tetrameric structure in an asymmetric unit of crystals. NADH not only acts as a proton donor, but also contributes to the stability of the α7 helix. This helix is a unique and functionally significant part of AtQR and is related to form a deep catalytic cavity. AtQR has all three catalytic residues of the short-chain dehydrogenases/reductases family and the hydrophobic wall for the enantioselective reduction of 3-quinuclidinone as well as RrQR. An additional residue on the α7 helix, Glu197, exists near the active site of AtQR. This acidic residue is considered to form a direct interaction with the amine part of 3-quinuclidinone, which contributes to substrate orientation and enhancement of substrate-binding affinity. Mutational analyses also support that Glu197 is an indispensable residue for the activity.

1. Introduction

Alzheimer's disease, the most common form of dementia, is a progressive degenerative illness characterized by continuing loss of memory, impaired cognition, and change in and loss of personality. Talsaclidine (WAL 2014 FU) is a nonselective muscarinic acetylcholine receptor agonist that acts as a full agonist of the M_1 subtype, and as a partial agonist of the M_2 and M_3 subtypes [1–3]. The compound is intended for muscarinic substitution therapy in patients with Alzheimer's disease. Talsaclidine appears to be a promising new candidate because even high doses cause only salivation as a side effect in healthy volunteers [4].

(*R*)-3-quinuclidinol is used as a chiral building block applicable to the synthesis of various pharmaceuticals including talsaclidine [5–9]. Chiral compounds are chemically synthesized by several chemical reactions, whereas 3-quinuclidinone reductase can easily synthesize (*R*)-3-quinuclidinol by the enantioselective reduction of 3-quinuclidinone. The enzyme was first isolated from *Rhodotorula rubra* (RrQR). RrQR requires NADPH as a cofactor and converts 3-quinuclidinone to (*R*)-3-quinuclidinol with a >99.9% enantiomeric excess [10]. Recently, a novel 3-quinuclidinone reductase was isolated from *Agrobacterium tumefaciens* (AtQR), which also produces the (*R*)-3-quinuclidinol with a >99.9% enantiomeric excess. Based on the amino acid sequence identity (43% identical to RrQR), AtQR belongs to the short-chain dehydrogenases/reductases (SDR) family like RrQR. However, AtQR requires only NADH as a cofactor. In addition, AtQR shows a 100 times higher substrate-binding affinity than RrQR [11], which indicates that AtQR is a more practical enzyme for application in the biosynthesis of (*R*)-3-quinuclidinol.

The structural analysis of AtQR would help us to elucidate the structural basis for its high substrate affinity and enantioselectivity, and contribute to the exploration on the general understanding of higher substrate affinity and enantioselectivity in enzymes. Here, we report the crystal structure of AtQR and its structural

* Corresponding author. Fax: +81 3 5841 8023.
E-mail address: amtanok@mail.ecc.u-tokyo.ac.jp (M. Tanokura).

http://dx.doi.org/10.1016/j.bbrc.2014.03.030
0006-291X/

difference from RrQR. Structural and mutational analyses were conducted to explain the high substrate-binding affinity and enantioselectivity.

2. Materials and methods

2.1. Protein expression, purification and crystallization

The recombinant AtQR was overexpressed as a fusion protein with an N-terminal His_6 tag in *Eschrichia coli* Rosetta(DE3) (Novagen) and purified by sequential chromatographies with Ni-NTA superflow (QIAGEN), DEAE Sepharose (GE Healthcare) and Hiload 26/60 superdex 200 prep grade (GE Healthcare) as previously described [12].

2.2. X-ray diffraction data collection and structure determination

For the crystallization of AtQR with its cofactor, 2 mM NADH was added to the protein solution. AtQR was crystallized under a reservoir solution condition of 0.2 M ammonium acetate, 0.1 M HEPES pH 8.5 and 24% (*w*/*v*) PEG3350 [12]. The X-ray diffraction data were collected on the BL-5A beamline at the Photon Factory (Tsukuba, Japan) using an ADSC Quantum 315r CCD detector. The diffraction data were indexed, integrated and scaled using *XDS* [13]. The crystal belonged to the primitive monoclinic space group $P2_1$, with unit-cell parameters of a = 62.0 Å, b = 126.4 Å, c = 62.0 Å and β = 110.5°.

2.3. Structure determination and refinement

We chose *meso*-2,3-butanediol dehydrogenase from *Klebsiella pneumonia* (PDB: 1GEG [14]) as a molecular replacement search model, because it also belongs to the SDR family and its sequence is the most similar to AtQR (43% identical) among the proteins whose structures are available. Molecular replacement was carried out using Phaser [15]. The initial model of AtQR was refined using the programs REFMAC5 and Coot [16,17]. The refinement statistics are summarized in Table 1.

2.4. Computational analysis

Molecular graphics were depicted using the program PyMOL (http://www.pymol.org). The solvent-accessible surface areas were calculated using AREAIMOL [18]. Hydrogen bonds with the NADH were calculated and depicted using LIGPLOT+ [19].

2.5. Site-directed mutagenesis

The expression plasmids for the mutants of AtQR were prepared using site-directed mutagenesis kit (Agilent Technologies). PCR was carried out with the expression plasmid for the wild-type AtQR, pET-28a(+)-AtQR, as template. Digestion with the restriction enzyme *Dpn*I was carried out at 37 °C for 1 h to remove the parent DNA, and the mutations were confirmed by DNA sequencing.

2.6. Enzyme activity measurements

Reductase activity was determined at 37 °C by measuring the decrease rate of NADH. The standard assay solution (2.5 ml) contains 618 μM 3-quinuclidinone-HCl, 320 μM NADH, 200 mM potassium phosphate buffer (pH 7.0) and the appropriate amount of the purified enzyme. After incubation for 2 min, the reaction was started by adding the enzyme. The absorbance at 340 nm was measured at 37 °C. The activity can be calculated from the decrease in absorbance. One unit of AtQR activity is calculated as the amount which oxidizes 1 μmol of NADH in 1 min.

Table 1
Data collection and refinement statistics.

	AtQR
Data collection	
Space group	$P2_1$
Cell dimensions	
a, *b*, *c* (Å)	62.0, 126.4, 62.0
α, β, γ (°)	90.0, 110.5, 90.0
Molecules/asymmetric unit	4
Wavelength (Å)	1.0000
Resolution (Å)[a]	20.0–1.72 (1.76–1.72)
R_{sym}[a,b]	4.3 (16.0)
$\langle I/\sigma(I)\rangle$[a]	21.7 (5.1)
Completeness[a]	97.9 (80.7)
Redundancy[a]	3.6 (1.8)
Refinement	
Resolution (Å)	19.8–1.72
R_{work}/R_{free}[c] (%)	15.0/18.3
No. Protein residues in monomers	257
No. non-protein atoms	
Ligand	132
Solvent	545
Others	20
Mean *B*-factor (Å^2)	14.9
Root mean square deviations	
Bond lengths (Å)	0.021
Bond angles (Å)	2.025
Ramachandran plot	
Most favorable (%)	97.2
Allowed (%)	1.9
Disallowed (%)	0.9

[a] Values in parentheses are for the highest resolution shell.
[b] $R_{sym} = \Sigma_{hkl}\ [(\Sigma_i\ |I_i - \langle I\rangle|)/\Sigma_i\ |I_i|]$, where I_i is the *i*th intensity measurement of reflection *hkl*, including symmetry-related reflections, and $\langle I\rangle$ is its average.
[c] The R_{free} factor was calculated using 5% of the reflections omitted from the refinement.

3. Results and discussion

3.1. Overall structure of AtQR

AtQR was overexpressed, purified and crystallized in the presence of the cofactor NADH. The crystal structure of AtQR was determined at 1.72 Å resolution and refined to a crystallographic *R*-factor of 0.150 and *R*-free of 0.183 (Table 1). Four protomers in an asymmetric unit formed a tetramer (Fig. 1A), in which only three protomers (chain A, B and C) formed complexes with NADH and the fourth protomer (chain D) showed an NADH-free structure. The root-mean-square deviations (r.m.s.d.) of chain A with chain B and chain C are 0.199 and 0.275 Å for the C^{α} atoms, respectively. The close r.m.s.d. values indicate that these protomers do not adopt large conformation changes while bound to NADH. In order to explain the structural feature of the NADH-bound form, we chose the chain C protomer because of its lowest overall *B*-factor (13.0 Å^2) among the three protomers (Table 2). As most other SDR family proteins, the protomer consists of two domains (Fig. 1B), a large domain and a small domain. The large domain is comprised of a typical Rossmann fold with a seven-stranded parallel β-sheet (β1–β7), which is flanked by seven α-helices (α1–α6 and α9) and four 3_{10}-helices (η1–η4) on both sides. The small domain contains two helices (α7 and α8) and protrudes from the globular body of the large domain. An NADH molecule was clearly observed in the cleft of the large domain (Fig. 1B and C). Meanwhile, the NADH-free protomer (chain D) can also be superimposed on chain A with an r.m.s.d. of 0.474 Å for the C^{α} atoms. Chain D shows almost the

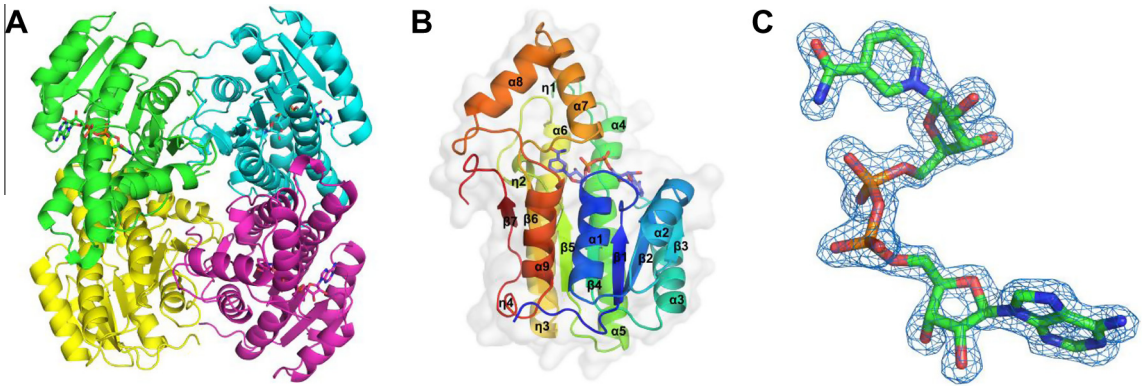

Fig. 1. (A) Quaternary structure of AtQR. The assembly of AtQR is a homotetramer, in which each protomer of AtQR is colored in green (chain A), cyan (chain B), magenta (chain C) or yellow (chain D). (B) Ribbon diagram of AtQR protomer bound to NADH (chain C). The ribbon is shown from blue (N-terminus) to red (C-terminus). NADH is shown as a stick model. (C) $2F_o - F_c$ electron density map of NADH is shown by the blue mesh that is contoured at 1.0σ.

Table 2
NADH-dependent 3-quinuclidinone reductase average *B*-factor.

	B-factor (Å^2)
Chain A	14.6
Chain B	14.3
Chain C	13.0
Residues 190–200 in chain C	15.9
Residues 190–200 in chain D	45.8

same backbone but with a slight shift of the α7 helix. The significance of this helix and the influence from the shift will be discussed later.

The homotetramer of AtQR is stabilized by three protein–protein interfaces (A–B, A–C, and A–D). The A–B interface consists of the two long helices: α9 and β7 and several loops. The buried area of the A–B interface is 3476 Å^2 per dimer, which is equivalent to 15.7% of the total surface area of the protomer. The A–D interface consists of α5 and α6 with a buried surface area of 3103 Å^2 per dimer (13.6% of the total surface area). In addition to these major interprotomer contacts, protomers A and C also make minor contacts with a buried surface area of 148 Å^2 (0.7% of the total surface area). These three interfaces are highly conserved among the SDR family proteins.

3.2. NADH-binding mechanism and NADH-induced conformational changes

NADH was located in a deep cleft of the large domain and bound at the C-terminal end of the β-sheet. The adenosine moiety of NADH was bound to a pocket formed by Gly16, Leu41, Val62, Asp63, Val64, Thr65, Ala91, Val93 and Val113 (Fig. 2A). The ribose ring of the adenosine moiety formed direct and water-mediated hydrogen bonds with the side-chain atoms of Asp40 and Lys19, respectively (Fig. 2A). In particular, Asp40 occupied the space for the additional phosphate moiety at the 2′-position of the ribose ring of the adenosine moiety. The residue is speculated to be the critical to the NADH selectivity of AtQR. The D40A mutant showed decreased enzymatic activity, which indicates that Asp40 plays an important role in binding to NADH (Table 3). The nicotinamide ring

Table 3
NADH-dependent 3-quinuclidinone reductase activity.

Enzyme	Activity
Wild type	100%
D40A	ND
R196A	76%
E197A	ND
Y216V	31%

ND, not detected.

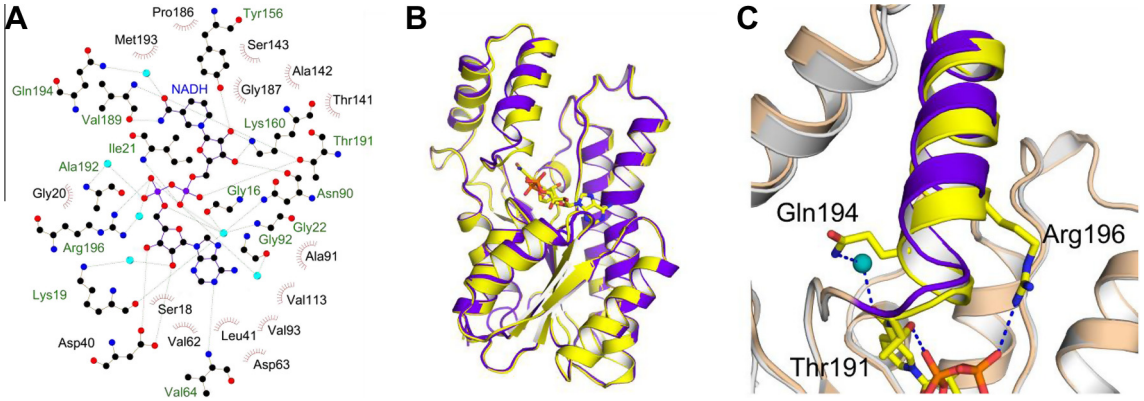

Fig. 2. (A) Schematic diagram for the non-covalent interactions between AtQR and NADH. The interactions were identified with the program LIGPLOT$^+$ [18]. (B) Superposition of structures between the ligand-free form and NADH-bound form. Chains C (NADH-bound) and D (ligand-free) are colored in yellow and purple-blue, respectively. (C) Interactions between NADH and the residues on the α7 helix. Residues interacting with NADH are represented by a stick model. Water molecule is shown by a sphere model.

contacted Ile21, Thr141, Ala142, Ser143, Phe186, Gly187 and Met193 through hydrophobic interactions, and the amide group formed hydrogen bonds with Val189 and Thr191 (Fig. 2A). The ribose ring connecting to the nicotinamide ring formed hydrogen bonds with the side-chain atoms of the residues Asn90, Tyr156 and Lys160 and hydrophobic interactions with Thr141 and Gly92 (Fig. 2A). The pyrophosphate moiety interacted with the main-chain atoms of Ile21, Thr191 and Arg196 (Fig. 2A).

Superimposition of chain C and chain D reveals that a small shift occurred on the α7 helix upon NADH binding (Fig. 2B). The average *B*-factors suggest that NADH binding also contributes to the stabilization of the α7 helix (residue 190–200) (Table 2). Some residues around the α7 helix interacted with NADH and contributed to the stabilization of the helix. Thr191 formed a hydrogen bond with the pyrophosphate moiety of NADH as mentioned above (Fig. 2A and C). Another residue Arg196 also interacted with the pyrophosphate moiety (Fig. 2C). R196A caused decreased activity, which indicates that the stabilization of the α7 helix contributes to the catalytic activity of AtQR (Table 3). In addition, the nicotinamide ring formed a hydrogen bond with the side chain of Gln194 through a water molecule. The conformational change upon NADH binding reveals that NADH not only acts as a hydride donor but also contributes to the stabilization of the α7 helix.

3.3. Comparison of overall structures with RrQR

Fig. 3A shows the superimposition of the AtQR and RrQR structures [20,21]. Although the overall structures of both enzymes are primarily identical (r.m.s.d. 4.198 for 231 C^{α} atoms), there are also three apparent differences. Firstly, AtQR does not possess the N-terminal region of RrQR, which contributes to the quaternary structure formation [20,21]. Secondly, the α7 helix in the small domain of AtQR is not conserved in RrQR (Fig. 3A). Thirdly, the entrances of substrate-binding pockets are different between AtQR and RrQR (Fig. 3B). In the structure of AtQR, the additional α7 helix occupies the space corresponding to the entrance of RrQR. However, the loop between the η2-helix and α6-helix of AtQR is shorter than that of RrQR, which enable the substrate to reach its active site.

3.4. Structural insight into high substrate-binding affinity and enantioselectivity

The catalytic mechanism of the SDR family enzymes has been well examined [22–24]. A catalytic triad of Ser-Tyr-Lys residues is conserved in the SDR family enzymes. The tyrosine residue functions as a catalytic base and abstracts a proton from the substrate. The serine residue plays a role in the stabilization of the bound substrate, and the lysine residue indirectly interacts with the hydroxyl of the tyrosine residue via the 2′-hydroxyl of the nicotinamide ribose of the cofactor and lowers its pK_a value. In the active site of AtQR, Ser143, Tyr156 and Lys160 are spatially conserved as the catalytic triad residues (Fig. 3C). In addition, the asparagine residue, which is important for the stabilization of the water molecule in the proton relay system [25], is also conserved as Asn114 in AtQR. AtQR also possesses two distinctive hydrophobic residues, Leu144 and Phe188, around the active site. The corresponding residues of RrQR (Ile167 and Phe212) were concluded to be a critical structural basis in relation to the hydrophobic wall for substrate recognition with direct hydrophobic interactions, which leads to the (*R*)-specific reaction. Therefore, high enantioselective reduction could be defined by this common structural basis of

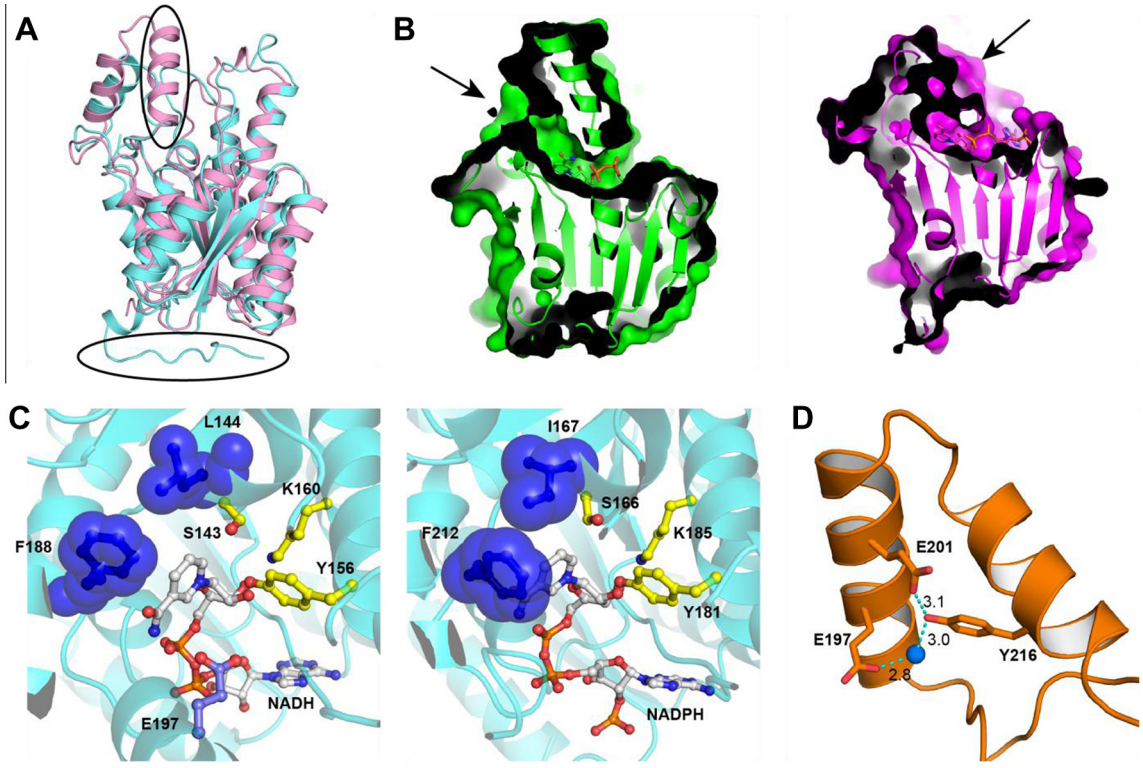

Fig. 3. (A) Superposition of AtQR and RrQR structures. Protein structures are shown by ribbon diagrams colored in pink for AtQR and aquamarine for RrQR. Circles show the different structural elements between the two enzymes. (B) Substrate entrances of AtQR (green) and RrQR (magentas). The entrances are indicated by arrows. (C) Active sites of AtQR (left) and RrQR (right). Catalytic-triad residues are colored in yellow. Residues forming the hydrophobic wall are highlighted by the stick-and-sphere model colored in blue. In the structure of AtQR (left), Glu197 is colored in slate. (D) Interactions between Tyr216 and α7 helix. Residues involved in the interactions are shown as sticks. Water molecule is shown by a sphere model. Hydrogen bonds are shown as dashed lines.

the 3-quinuclidinone reductases. In addition, AtQR also has a distinctive residue Glu197 that orients towards the substrate-binding site (Fig. 3C). The E197A mutant showed no activity, which indicates that Glu197 is related to the reductase activity as a non-catalytic residue (Table 3). It is speculated that the Glu197 improves the binding affinity of 3-quinuclidinone by forming a salt bond with its tertiary amine. The binding could also induce 3-quinuclidinone to a certain orientation which is favorable for proton transfer. Additionally, Glu197 belongs to the α7 helix and is not conserved in RrQR. Therefore, Glu197 may be the key residue for enhancing the substrate-binding affinity. Tyr216 interacts with Glu201 of the α7 helix and also forms a hydrogen bond with Glu197 through a water molecule (Fig. 3D). The Y216V mutation causes decreased activity, which supports that the orientation of Glu197 is important for the substrate binding (Table 3).

3.5. Conclusion

We provide the crystal structure of the 3-quinoclidinone reductase AtQR in both the NADH-bound state and NADH-free state. Structural comparison between the two states revealed that the co-factor NADH not only acts as a proton donor, but also contributes to the stabilization of the α7 helix that is not conserved in RrQR. Although the catalytic triad of the SDR family and the hydrophobic wall are well conserved in both AtQR and RrQR, a critical residue, Glu197, located at the additional α7 helix in AtQR, is found near the active site and confirmed to be activity-related. Therefore, the Glu197 is considered to be the residue that is critical to the high activity. Based on these findings, we conclude that the stabilization of the α7 helix contributes to the high activity by orienting a critical residue Glu197 to the active site.

3.6. Accession numbers

The atomic coordinate and structure factor of AtQR have been deposited to Protein Data Bank (PDB) with accession code 3WDS.

Acknowledgments

We would like to thank the beamline staff at Photon Factory. The synchrotron radiation experiments were performed at BL5A in the Photon Factory, Tsukuba, Japan (Proposal No. 2008S2-001). This research is supported by the Targeted Proteins Research Program (TPRP) of the Ministry of Education, Culture, Sports, Science, and Technology (MEXT), Japan.

References

[1] H.A. Ensinger, H.N. Doods, A.R. Immel-Sehr, F.J. Kuhn, G. Lambrecht, K.D. Mendla, R.E. Müller, E. Mutschler, A. Sagrada, G. Walther, WAL 2014–a muscarinic agonist with preferential neuron-stimulating properties, Life Sci. 52 (1993) 473–480.
[2] A. Walland, S. Burkard, R. Hammer, W. Tröger, In vivo consequences of M_1-receptor activation by talsaclidine, Life Sci. 60 (1997) 977–984.
[3] M. Wienrich, D. Meier, H.A. Ensinger, W. Gaida, A. Raschig, A. Walland, R. Hammer, Pharmacodynamic profile of the M_1 agonist talsaclidine in animals and man, Life Sci. 68 (2001) 2593–2600.
[4] W.S. Adamus, J.P. Leonard, W. Tröger, Phase I clinical trials with WAL, a new muscarinic agonist for the treatment of Alzheimer's disease, Life Sci. 56 (1995) (2014) 883–890.
[5] M. Takeuchi, R. Naito, M. Hayakawa, Y. Okamoto, Y. Yonetoku, K. Ikeda, Y. Isomura, Novel quinuclidine derivatives and medicinal composition thereof, European patent EP 0801067 (1996).
[6] V.A. Alabaster, Discovery & development of selective M_3 antagonists for clinical use, Life Sci. 60 (1997) 1053–1060.
[7] J.S. Ward, L. Merritt, D.O. Calligaro, F.P. Bymaster, H.E. Shannon, C.H. Mitch, C. Whitesitt, D. Brunsting, M.J. Sheardown, P.H. Olesen, M.D. Swedberg, L. Jeppesen, P. Sauerberg, 1,2,5-Thiadiazole analogues of aceclidine as potent M_1 muscarinic agonists, J. Med. Chem. 41 (1998) 379–392.
[8] A. Leusch, W. Tröger, A. Greischel, W. Roth, Pharmacokinetics of the M_1-agonist talsaclidine in mouse, rat, rabbit and monkey, and extrapolation to man, Xenobiotica 30 (2000) 797–813.
[9] T. Ishihara, H. Kakuta, H. Moritani, T. Ugawa, I. Yanagisawa, Synthesis and biological evaluation of quinuclidine derivatives incorporating phenothiazine moieties as squalene synthase inhibitors, Chem. Pharm. Bull. (Tokyo) 52 (2004) 1204–1209.
[10] A. Uzura, F. Nomoto, A. Sakoda, Y. Nishimoto, M. Kataoka, S. Shimizu, Stereoselective synthesis of (*R*)-3-quinuclidinol through asymmetric reduction of 3-quinuclidinone with 3-quinuclidinone reductase of *Rhodotorula rubra*, Appl. Microbiol. Biotechnol. 83 (2009) 617–626.
[11] S. Shimizu, M. Kataoka, F. Nomoto, A. Uzura, Alcohol dehydrogenase, gene encoding the same and method for producing optically active (*R*)-3-quinuclidinol using the same, Japanese Patent 2008-212144 (2008).
[12] F. Hou, T. Miyakawa, D. Takeshita, M. Kataoka, A. Uzura, K. Nagata, S. Shimizu, M. Tanokura, Expression, purification, crystallization and X-ray analysis of 3-quinuclidinone reductase from Agrobacterium tumefaciens, Acta Crystallogr, F Struct. Biol. Cryst. Commun. 68 (2012) 1237–1239.
[13] K. W., Automatic processing of rotation diffraction data from crystals of initially unknown symmetry and cell constants, J. Appl. Crystallogr. 26 (1993) 795–800.
[14] M. Otagiri, G. Kurisu, S. Ui, Y. Takusagawa, M. Ohkuma, T. Kudo, M. Kusunoki, Crystal structure of meso-2,3-butanediol dehydrogenase in a complex with NAD+ and inhibitor mercaptoethanol at 1.7 A resolution for understanding of chiral substrate recognition mechanisms, J. Biochem. 129 (2001) 205–208.
[15] A.J. McCoy, R.W. Grosse-Kunstleve, P.D. Adams, M.D. Winn, L.C. Storoni, R.J. Read, Phaser crystallographic software, J. Appl. Crystallogr. 40 (2007) 658–674.
[16] G.N. Murshudov, A.A. Vagin, E.J. Dodson, Refinement of macromolecular structures by the maximum-likelihood method, Acta Crystallogr D Biol Crystallogr 53 (1997) 240–255.
[17] P. Emsley, K. Cowtan, Coot: model-building tools for molecular graphics, Acta Crystallogr. D Biol. Crystallogr. 60 (2004) 2126–2132.
[18] B. Lee, F.M. Richards, The interpretation of protein structures: estimation of static accessibility, J. Mol. Biol. 55 (1971) 379–400.
[19] R.A. Laskowski, M.B. Swindells, LigPlot+: multiple ligand-protein interaction diagrams for drug discovery, J. Chem. Inf. Model. 51 (2011) 2778–2786.
[20] D. Takeshita, M. Kataoka, T. Miyakawa, K. Miyazono, S. Kumashiro, T. Nagai, N. Urano, A. Uzura, K. Nagata, S. Shimizu, M. Tanokura, Structure basis of stereospecific reduction by quinuclidinone reductase, AMB Express 4 (2014) 6.
[21] D. Takeshita, M. Kataoka, T. Miyakawa, K. Miyazono, A. Uzura, K. Nagata, S. Shimizu, M. Tanokura, Crystallization and preliminary X-ray analysis of the NADPH-dependent 3-quinuclidinone reductase from *Rhodotorula rubra*, Acta Crystallogr. F Struct. Biol. Cryst. Commun. 65 (2009) 645–647.
[22] H. Jörnvall, B. Persson, M. Krook, S. Atrian, R. Gonzàlez-Duarte, J. Jeffery, D. Ghosh, Short-chain dehydrogenases/reductases (SDR), Biochemistry 34 (1995) 6003–6013.
[23] C. Filling, K.D. Berndt, J. Benach, S. Knapp, T. Prozorovski, E. Nordling, R. Ladenstein, H. Jörnvall, U. Oppermann, Critical residues for structure and catalysis in short-chain dehydrogenases/reductases, J. Biol. Chem. 277 (2002) 25677–25684.
[24] D. Ghosh, M. Sawicki, V. Pletnev, M. Erman, S. Ohno, S. Nakajin, W.L. Duax, Porcine carbonyl reductase. structural basis for a functional monomer in short chain dehydrogenases/reductases, J. Biol. Chem. 276 (2001) 18457–18463.
[25] K. Kubota, K. Nagata, M. Okai, K. Miyazono, W. Soemphol, J. Ohtsuka, A. Yamamura, N. Saichana, H. Toyama, K. Matsushita, M. Tanokura, The crystal structure of l-sorbose reductase from *Gluconobacter frateurii* complexed with NADPH and l-sorbose, J. Mol. Biol. 407 (2011) 543–555.